Research on Key Technologies for Radionuclide Removal via Steel-slag Two-phase Reaction during Smelting

Authors: Zhao, Dr. mu, Lu, Dr. Tiezhong, Prof. Xuan Zhao, Zhao, Dr. Mu

Date: 2025-11-21T00:00:00+00:00

Abstract

This study systematically investigates smelting decontamination technology and recycling strategies for radioactively contaminated steel. The decontamination process involves both the crystalline and molten phases, where the molten stage facilitates the complexation of decontaminants with radionuclides at elevated temperatures, promoting radionuclide partitioning into the slag or dust phase. Research focuses on elucidating the mechanisms of smelting decontamination, optimizing hybrid smelting processes, and analyzing the characteristics of the slag-steel system. The findings reveal that smelting decontamination is fundamentally a thermodesorption process, with radionuclide partitioning efficiency governed by their oxygen affinity. For steel contaminated with artificial radionuclides, hybrid smelting technology significantly enhances recycling efficiency. The dosage of decontaminant requires careful optimization, weighing decontamination efficiency against secondary waste generation. The resultant slag exhibits a honeycomb-like or porous structure, with its surface morphology closely correlated to its chemical composition.

Full Text

Preamble

Research on Key Technologies for Radionuclide Removal via Steel-Slag Two-Phase Reaction During Smelting

Mu Zhao[1,3], Tiezhong Lu[2], Xuan Zhao[1]
[1]Institute of Nuclear and New Energy Technology, Tsinghua University, Beijing 100084, China
[2]China National Nuclear Power Co., Ltd, Beijing 100089, China
[3]China Nuclear Industry 24 Construction CO., LTD., Hebei Yanjiao 101601, China

Abstract: This study systematically investigates decontamination technologies and recycling strategies for radioactively contaminated steel. The decontamination process involves both crystalline and molten phases, where the molten stage facilitates complexation of decontaminants with radionuclides at elevated temperatures, promoting radionuclide partitioning into the slag or dust phase. Research focuses on elucidating smelting decontamination mechanisms, optimizing hybrid smelting processes, and analyzing characteristics of the slag-steel system. Findings reveal that smelting decontamination is fundamentally a thermodesorption process, with radionuclide partitioning efficiency governed by oxygen affinity. For steel contaminated with artificial radionuclides, hybrid smelting technology significantly enhances recycling efficiency. The decontaminant exhibits a honeycomb-like or porous structure, with surface morphology closely correlated to chemical composition.

Keywords: Smelting; Two-phase reaction; Oxygen affinity; Slag

1. Introduction

Radioactively contaminated steel is primarily generated from nuclear facilities, radioactive sources, and radiation devices during operation and decommissioning. The main types of such waste are contaminated materials formed by radionuclides carried by media and trapped on steel surfaces. The decontamination process for radioactive steel predominantly involves two distinct phases: the crystalline phase and the molten state. Within the molten phase, volume reduction and reshaping of the steel bulk are achieved, while this stage also serves as the primary mechanism for deep decontamination.

Smelting technology entails introducing decontaminants into the smelting furnace, where they undergo co-melting with radioactively contaminated steel. Elevated temperatures facilitate complexation reactions between decontaminants and contaminating radionuclides, promoting partitioning of the majority of radionuclides into the slag phase or fume dust phase, thereby purifying the steel bulk. After smelting, residual radionuclides within the steel exist in a homogeneous and stable state of incorporation. The efficacy of the smelting decontamination process is significantly influenced by the physicochemical properties of the decontaminants. Transuranic elements, being highly oxidation-prone, exhibit pronounced enrichment within the slag phase. Conversely, artificial radioactive nuclides exhibiting -decay, such as cobalt (Co), nickel (Ni), chromium (Cr), zinc (Zn), and manganese (Mn), demonstrate significant limitations in decontamination efficiency.

This study investigates hybrid smelting of radioactively contaminated steel, focusing on elucidating migration and transformation mechanisms of radionuclides and evaluating characteristic parameters and yield of the resultant smelting slag.

2. Experimental

Prior to furnace ignition, radioactive testing must be conducted on the lining of the medium-frequency furnace. For each batch of material preparation, radioactively contaminated steel suitable as smelting feedstock shall be selected based on dose control requirements of the target product. The decontaminant shall be prepared according to process formulation, with its minimum addition quantity controlled under the premise of ensuring decontamination efficacy, and processed into well-dispersed particles with a particle size of 0.5–3 mm before use.

During operation, the decontaminant shall first be added to the furnace bottom at 30%–50% of the formulation amount. This practice not only extends contact time between the decontaminant and radionuclides to enhance decontamination efficiency but also protects the furnace bottom and facilitates pre-slagging. After each subsequent addition of decontaminant, an interval of at least 15–20 minutes shall be maintained for slag skimming and related operations.

When the temperature of radioactively contaminated steel in the furnace rises to 1000°C–1300°C, the furnace temperature shall be stabilized to maintain a partially melted state (to avoid excessive melting). Subsequently, low-pressure oxygen shall be introduced onto the surface of the molten steel. During the oxygen-blowing process, pressure must be strictly controlled to prevent overpressure while ensuring a continuous oxygen supply time of 30 minutes. After ceasing oxygen blowing, the input power of the medium-frequency furnace shall be gradually increased to approximately 70%. As the lower radioactively contaminated steel gradually melts, stirring the charge shall assist in smelting. Secondary charging shall be performed when the melting rate of the charge reaches 70%–80%.

After the radioactively contaminated steel is completely melted, the molten pool shall be fully stirred, high-efficiency slag remover shall be added, and slag skimming shall be conducted. The resulting steel slag shall be temporarily stored in 200L standard steel drums. After complete smelting of all feedstock, the furnace temperature shall be elevated and stabilized at 1560°C–1580°C. Deoxidizers such as ferrosilicon alloy and aluminum shall be added according to process requirements to complete the deoxidation process, followed by tapping and casting.

Characterization of steel and slags was performed using built-in Energy-dispersive X-ray Analysis (EDS, HORIBA EX 350i). Raman spectroscopy was conducted using a Witec RISE system with a 532 nm laser wavelength. Scanning Electron Microscopy (SEM, SU8020) was also employed.

3. Results and Discussion

3.1 Mechanism of Decontaminant in Decontamination

The smelting decontamination of radioactively contaminated steel is essentially a thermodesorption process—driven by thermal energy, pollutants adsorbed in the molten steel medium are facilitated to dissociate or volatilize. Subsequently, based on physicochemical properties of different elements and their radioactive isotopes, these pollutants achieve redistribution among the slag phase, molten steel, and exhaust gas phases. The decontaminant plays a critical role, primarily enhancing pollutant removal efficiency through its complexation effect on impurities in molten steel.

Similar to non-metallic inclusions in molten steel, radionuclides combine with oxygen and form slag phase under the action of flux. Due to the liquid state of slag and its density difference from molten steel, effective separation is readily achievable. Specifically, high-melting-point radionuclides require existence in oxide form to efficiently enter the slag phase and undergo complexational extraction by the flux; whereas low-boiling-point/low-melting-point radionuclides (e.g., Cs, C, H) may either escape into exhaust gas with carbon monoxide (CO) bubbles during molten steel boiling or remain residual in the furnace lining.

The removability of radionuclides represented by uranium (U) and Co from molten steel via smelting primarily depends on their oxygen affinity. The oxidation of radionuclides mainly relies on iron monoxide (FeO) as the oxidizing agent. From a thermodynamic perspective, whether radionuclide (M) can efficiently enter the slag phase depends on the relationship between Gibbs free energy difference (ΔG) and reaction equilibrium constant (Kc) between M oxide and FeO. During smelting, the following redox reaction may occur between Fe and M oxides:

$$yFe + M_xO_y \rightleftharpoons xM + yFeO \qquad (1)$$

The equilibrium constant (Kc) is:

$$K_c = \frac{c^y(Fe) \cdot c(FeO)}{c(M_xO_y) \cdot c^x(M)} = e^{[(2\Delta G(M_xO_y) - 2\Delta G(FeO))/RT]} \qquad (2)$$

where: c = equilibrium molar fraction (mol); ΔG = Gibbs free energy of oxide formation ($J \cdot mol^{1}$); R = universal gas constant, 8.28×10^{3} $J \cdot mol^{1} \cdot K^{1}$; T = temperature (K).

Based on thermodynamic relationships involving enthalpy (H), entropy (S), and temperature (T), Gibbs free energy (ΔG) serves as an effective criterion for determining chemical reaction equilibrium direction. When 2ΔG(M_xO_y) - 2ΔG(FeO) > 0 (i.e., reaction equilibrium constant Kc > 1), Reaction (1) proceeds forward. In this case, radionuclides (M) exist as oxides and are complexationally extracted by the decontaminant into the slag phase. Conversely, if Kc

< 1, Reaction (1) proceeds in reverse, leaving M in elemental state that cannot be complexed by the decontaminant, resulting in decontamination failure.

U exhibits stronger oxygen affinity than Fe, leading to significant decontamination efficiency. U forms slag phases covering the molten steel surface through complexation with CaO and CaF , existing in forms such as uranyl complexes (UO , UO SO ², UO (SO) ², UO (SO) , UO Cl , UO Cl , UO NO). U can embed into silicate anions (e.g., Si O , Si O ¹²) to form a U-O-Si three-dimensional network. U readily generates UO ², which reduces mobility through hydrogen bonding or electrostatic interactions with silicate anions. A portion of UO ² is encapsulated within crystal defects of $2CaO \cdot SiO$, immobilized as solid solutions or precipitates. Additionally, UO ² can react with free O² to form uranyl precipitates such as CaUO .

Isotopes such as Co and ³Ni, which exhibit properties similar to Fe, are challenging to remove via conventional smelting. Their distribution among steel ingots, slag, and fume is determined by thermodynamic equilibrium. Although cobalt oxides can be captured by slag, their lower thermodynamic stability compared to iron oxide ($Kc < 1$) prevents Reaction (1) from proceeding forward, making cobalt oxide formation difficult and limiting the decontaminant' s efficacy. Thus, high-temperature crystallographic phase temperature gradient decontamination technology achieves phase-specific oxidation and initial decontamination, followed by molten-phase complexation decontamination.

Cobalt in the slag mainly exists in three forms: (1) At high temperatures, Co O decomposes into CoO, which reacts with basic fluxing agents (CaO, SiO , residual P O) to form stable compounds (e.g., CoSiO , CaCoO , Co (PO)) in the slag phase. The upward flotation of silicate slag further promotes the forward reaction by reducing CoO activity. (2) Non-oxidized cobalt is physically entrained and removed with the slag. (3) A small amount of free Co² embeds into silicate anion networks (e.g., Si O , Si O ¹²), forming Co-O-Si bonds and becoming encapsulated by the silicate network.

3.2 Analysis of Co-Smelting with Different Dose Steels

During decommissioning of a million-kilowatt pressurized water reactor (PWR), approximately 7,000 tons of medium- to low-level radioactive contaminated steel are generated. Activated corrosion products deposited on inner walls of the primary coolant system and related auxiliary pipelines primarily contain nuclides such as Co, Co, Mn, Fe, Zr, and ¹² Sb. Among these, Co dominates the inner walls of main system pipelines, originating primarily from cobalt in reactor coolant pressure boundary alloy materials and degradation of cobalt in stellite hardfacing of wear-resistant components (e.g., valves and pump shafts). This nuclide contributes approximately 70% of the total dose, simplifying regulatory dose requirements to focus on the Co dose limit.

During large-scale smelting, complete separation from slag is challenging, potentially leaving small Co-containing steel pellets in the slag. This results in

elevated radioactive levels in the slag, with Co being the primary contributing nuclide. Generally, surface-contaminated steel from cooling system pipelines, steam generator heat transfer tubes, and pump/valve components can be recycled via smelting; however, neutron-activated bulk contaminated steel from components such as the reactor pressure vessel, core internals, and biological shielding is often subjected to geological disposal. Activated steel, characterized by high radioactivity and uniform nuclide distribution, cannot meet recycling requirements through simple smelting alone. By co-smelting it with decontaminated low-level contaminated steel, synergistic recycling of surface-contaminated steel and activated steel can be achieved. Ultimately, the specific activity of charged steel must be reverse-calculated based on product dose requirements to ensure it falls below the permitted limit.

The mass percentage composition of decontaminant is: 20%-26% CaO, 5%-15% MgO, 3%-8% CaF , 5%-15% Fe O , 30%-40% SiO , and 7%-15% Al O . Smelting decontamination with this agent reduces contamination levels by 10%-30%.

Mixed smelting of activated steel and low pollution steel

Weight activated Steel	Specific activity of activated steel (Bq/g)	Weight low-dose steel	Specific activity of low-dose steel (Bq/g)	Weight charged furnace	Specific activity of charged material (Bq/g)	Weight tapped furnace	Specific activity of tapped material (Bq/g)	Decontamination efficiency	Recycling
24.08%	31.39%	20.87%	94.90%	94.71%	93.06%				

As shown in Table 1, steel may contain non-metallic impurities and desulfurizer-entrapped materials before smelting. The weight of steel out of the furnace is reduced compared with that of steel put into the furnace, but its recycling rate exceeds 90%. Low-dose steel (with a specific activity of 0.045 Bq/g) falls under decontrolled contaminated steel. Through smelting, homogenization of contaminated nuclides and material reshaping can be achieved without requiring additional decontaminant addition. In cases where activated steel is incorporated, achieving decontrol only necessitates the addition of 0.444 kg of activated steel. In Experiment 3, when the addition amount of activated steel was increased to 126.395 kg, the specific activity of tapped material decreased to 17.48 Bq/g, complying with the limit requirement specified in the "Notice on Strengthening Radiation Safety Supervision of Enterprises Engaged in Recycling and Smelting of Scrap Metal" issued by the former Ministry of Environmental Protection of China, which states that materials with specific activity below 20 Bq/g may be recycled for reuse under supervision of local environmental protection departments.

3.4 Analysis of Post-Smelting Steel-Slag

Figure 1 presents SEM images of post-smelting stainless steel and corresponding surface element distribution. As observed, the steel surface exhibits slag pits and microcracks, with residual radionuclides displaying uniform distribution characteristics within the steel ingot matrix. Notably, the activity of Co reaches 0.036 Bq/g, which satisfies radioactive decontrol criteria.

Post-smelting steel composition

Element	Elemental composition of steel after smelting (%)	Elemental composition of typical 304 steel (%)
C	0.08	0.08
O	0.002	0.002
Mg	0.001–0.005	0.001–0.005
Al	0.01–0.10	0.01–0.10
S	1.0	1.0
Ca	0.030	0.030
Fe	0.001–0.005	0.001–0.005
Cr	18.0–20.0	18.0–20.0
Ni	60-70	60-70
Other	8.0–11.0	8.0–11.0

Compared with typical 304 stainless steel, post-smelting steel demonstrates significantly higher mass fractions of elements such as C, O, Mg, Al, S, and Ca. These elevated elemental contents result in increased hardness, reduced impact toughness, and diminished fatigue resistance of post-smelting steel, rendering it unsuitable for use as high-strength structural material. Nevertheless, its metallic properties can still be fully utilized, prioritizing applications in products such as steel drums, steel boxes, and steel shots.

During the smelting process, radioactive slag floats up to the surface of molten steel and upon cooling forms high-hardness bulk agglomerates. Its surface exhibits two typical morphologies: hard smooth regions and rough porous regions.

FIGURE:2 presents a transmission SEM image of slag after crushing and rough grinding. The surface of rough regions displays a gray uneven arrangement interspersed with deep pores tens of micrometers in size, while smooth regions appear grayish-white. Figure 2(b) shows radioactive dust collected on the filter screen, which initially exists as black powdery micrometer-sized fine particles.

As shown in FIGURE:3, the overall surface of radioactive slag appears as a honeycomb-like grayish-black solid. FIGURE:3 reveals that its local surface exhibits a colorless glassy state, primarily composed of silicate compounds (e.g., Si O and Si O ^{12}). In this region, Si and O atoms are connected via covalent bonds to form a silicon-oxygen framework. Fe-O-Si bonds encapsulate

Fe^{2} within the silicate network, creating non-reactive zones that result in lower decontamination efficiency of the decontaminant in this area.

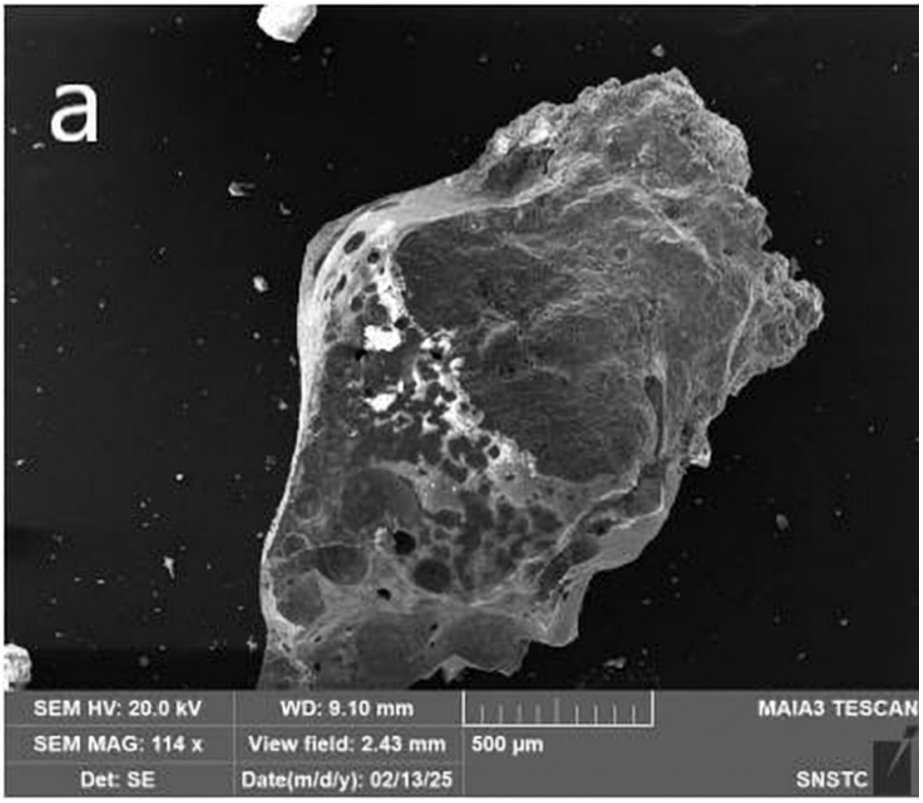

Figure 1: Figure 4

shows the EDS spectrum of radioactive slag after smelting. The color of smelting waste slag from radioactively contaminated steel ranges from grayish-white to grayish-black, with these variations primarily determined by a combination of chemical composition, phase structure, and radionuclide distribution. Specifically, CaO is inherently white, while pure SiO exists as a colorless crystal; when composite compounds such as CaSiO and CaAl O form within the slag, the overall color shifts to grayish-white. If the slag contains higher concentrations of impurities such as Fe and Mn, it manifests as gray.

The surface morphology of slag is categorized into three distinct regional types: - **Region 1 (grayish-white):** Exhibits a relatively flat and smooth surface, with EDS analysis indicating high content of Fe and Ca elements. - **Region 2 (outer grayish-black stone-like structure):** Displays a smooth surface and is characterized by high Si content based on EDS results. - **Region 3 (outermost grayish-black region):** Features a concave-convex grooved texture on

its surface and an internal grid-like skeletal structure.

In Region 1, Ca^{2} ions disrupt the silicon-oxygen network, forming SiO tetrahedra. This disruption increases internal porosity of the slag, reduces its viscosity, and enhances oxygen transport capacity. Under high-temperature conditions, Co O decomposes into CoO. Free CoO readily reacts with basic components in the slag (e.g., CaO, SiO , P O) to form stable compounds such as CoSiO , CaCoO , or Co (PO) , thereby enriching radionuclides within the slag phase. Additionally, a small amount of free Co^{2} embeds into the three-dimensional network structure formed by Si O and Si O ^{12} ions, binding with the silicon-oxygen network via Co-O-Si bonds and becoming encapsulated. Region 3 is a non-reactive zone where dense three-dimensional networks are formed by Si O and Si O ^{12} ions. The bound FeO in this region exhibits low oxygen potential, and the encapsulating effect of the silicon-oxygen network significantly hinders contact between FeO and the molten steel interface, deteriorating kinetic conditions for oxidation reactions. In Region 1, flowing slag gradually infiltrates gaps within the three-dimensional network, and upon cooling, solidifies into a hard, honeycomb-like structure. Region 2, acting as a transitional zone, exhibits semi-reactive characteristics. After flowing slag fully infiltrates and densifies the three-dimensional network, it ultimately forms a compact and rigid solid.

3.5 Analysis of Slag Generation

Dust and waste slag generated during smelting decontamination exhibit high concentrations of radionuclides, concomitant with elevated disposal costs. The core objective of smelting decontamination is to enhance efficiency by increasing radioactive dosage in slag while maintaining consistent specific activity of contaminated steel, simultaneously minimizing slag mass to reduce disposal costs. The composition and dosage of decontaminant must be determined based on radionuclide type and contamination level. Generally, lower decontaminant quantities are required for smelting low-level contaminated radioactive steel compared to high-level contaminated steel.

Specifically, when contaminant radionuclides exhibit strong oxidation potential, the decontaminant demonstrates higher efficiency, broader component selectivity, and reduced dosage requirements. Conversely, when oxidation potential is weaker, decontaminant efficiency decreases. Although increasing decontaminant dosage can improve effectiveness, this approach leads to substantial increases in waste slag volume, necessitating integration of high-efficiency pretreatment techniques for collaborative decontamination. Rational control of slag mass contributes to enhanced outcomes; however, merely increasing slag volume not only fails to effectively promote radionuclide removal but also exacerbates secondary waste generation. Therefore, selection of high-efficiency decontaminants represents a superior solution.

When the mass of U-contaminated steel is 250 kg, [FIGURE:5] illustrates the relationship between decontaminant dosage (expressed as mass percentage of

contaminated steel) and corresponding decontamination efficiency and slag generation amount at dosages of 0.25%, 0.5%, 1%, 1.5%, 2%, and 3%. As shown in Figure 5, decontaminant dosage exhibits a significant positive correlation with slag generation amount, indicating that reducing decontaminant usage can effectively mitigate secondary waste production. Regarding decontamination efficiency trend, it first increases then decreases with rising dosage, though overall reduction remains relatively minor, demonstrating excellent decontamination performance toward natural radionuclides. Notably, at 1% dosage, decontamination efficiency reaches 98%, with slag generation accounting for approximately 3% of contaminated steel mass. This dosage represents an optimal addition ratio balancing effective decontamination with secondary waste control.

When the mass of artificially contaminated steel is 250 kg, [FIGURE:6] illustrates the relationship between decontaminant dosage and corresponding decontamination efficiency and slag generation amount at dosages of 0.5%, 1%, 2%, 3%, 4.5%, and 6%. As shown in Figure 6, both efficiency and slag generation exhibit positive correlation with dosage: beyond 3%, the rate of efficiency increase slows significantly, whereas slag generation rises rapidly. Therefore, a dosage of 4.5%—yielding 28% decontamination efficiency and approximately 6% slag generation—is identified as a preferable option balancing effectiveness with waste control. Notably, the radioactively contaminated steel underwent high-temperature crystallographic phase temperature gradient decontamination pretreatment prior to smelting, which significantly enhanced efficiency, though thermodynamic limitations still constrain performance. During smelting decontamination, minimizing slag generation is critical. Decontaminant selection must balance improvements in steel quality. During melting, promoting uniform radionuclide distribution within molten steel effectively reduces formation of localized high-dose "hot spots," thereby lowering overall radiation dose.

4. Conclusions

This study conducts a systematic investigation into smelting decontamination technology for radioactively contaminated steel. Through experimental verification and theoretical analysis, it reveals core mechanisms underlying smelting decontamination, validates feasibility of co-smelting technology, and identifies key parameters for optimizing decontaminants. These findings provide theoretical support and technical references for radioactive waste management. Future research may develop novel composite decontaminants targeting low-oxygen-affinity nuclides (e.g., Co), construct nuclide migration prediction models, and explore novel processes such as smelting-electrolysis coupling. These advancements aim to enhance decontamination efficiency, reduce secondary waste generation, and promote resource utilization of radioactively contaminated steel and development of a circular economy.

5. Acknowledgments

This project has been supported by the "Research and Engineering Demonstration Project of Collaborative Decontamination and Control Technology and Equipment for Radioactively Contaminated Metal Materials" (2019YFC1907704), funded by the National Key Research and Development Program.

References

[1] Dacquait F, Francescatto J, Tevissen E, et al. Simulation of Co-60 uptake on stainless steel and alloy 690 using the OSCAR v1.4 code integrating an advanced dissolution-precipitation model[J]. Nuclear Engineering and Design, 2023, 405:112190.
[2] Zhao M, Fan Z et al. Overall consideration on the development of specialized complete sets of equipment for decommissioning of early aged nuclear facilities. Nuclear Safety, 2021, 81(4):66-71.
[3] Ma Y, Huang B, Chen J, et al. Deposition behavior of corrosion products in an ITER water-cooling experimental loop[J]. Fusion Engineering and Design, 2020, 159:111883.
[4] Dekker L., Osborne T. H., Santini J. M. Isolation and identification of cobalt- and caesium-resistant bacteria from a nuclear fuel storage pond. FEMS Microbiol Lett. 2014;359(1):81-4.
[5] M. Zhao, Y.F. Hua, et al. One-stop novel decontamination melting and reuse method for radioactively contaminated steel scrap. China Patent: ZL 2022 1 0834870.3. 2022-07-15.
[6] Mu Zhao, Yunfei Hua, et al. Comprehensive considerations for the co-decontamination and recycling of radioactively contaminated steels[J]. Nuclear Engineering and Design, 2025, 435:113945.
[7] Ohashi T, Ito T, Hosokawa H, et al. Investigation of cobalt buildup behavior and suppression by zinc injection on stainless steel under HWC conditions using simultaneous continuous measurements of corrosion and cobalt buildup[J]. Journal of Nuclear Science and Technology, 2015, 52(4):588-595.
[8] Cantatore V, Geers C, Chen J, et al. Insights into the zinc effect on radio-cobalt deposition on stainless steel piping surfaces under BWR conditions from experiment guided 1st principles modelling[J]. Journal of Nuclear Materials, 2020, 540:152361.
[9] Tigeras A, Bachet M, Catalette H, et al. PWR iodine speciation and behaviour under normal primary coolant conditions: An analysis of thermodynamic calculations, sensibility evaluations and NPP feedback[J]. Progress in Nuclear Energy, 2011, 53(5):504-515.
[10] Jian Deng, Jieheng Lei, Guolong Wang, Lin Zhong, Mu Zhao and Zeyong Lei. Experimental investigation of cobalt deposition on 304 stainless steel in borated and lithiated high-temperature water. Materials, 2023, 16(10):3834.
[11] Kim G N, Lee M W, Park H M, et al. Abrasive Blasting Technology for Decontamination of the Inner Surface of Steam Generator Tubes[J]. Nuclear

Engineering and Technology, 2011, 43(5):469-476.
[12] Lin Zhong, Jian Deng, Zhe-wen Zuo, et al. Simulation analysis and evaluation of decontamination effect of different abrasive jet process parameters on radioactively contaminated metal. Nuclear Engineering and Technology, 2023, 55(11):3940-3955.
[13] M. Zhao, J.H. Lei, et al. A method and device for removing radioactive metal solid phase temperature difference cascade. China Patent: ZL 202311710560.1. 2023-12-11.
[14] Wang Xiaoxia, Li Zhuoran, Zhang Liying, You Wei, Liu Song, Mi Aijun, Mao Yawei, Gao Guiling. Analysis of primary coolant corrosion product effect on solid waste source term. International Conference on Nuclear Engineering. 2017.
[15] Holdsworth S, Scenini F, Burke M G, et al. The effect of high-temperature water chemistry and dissolved zinc on the cobalt incorporation on type 316 stainless steel oxide[J]. Corrosion Science, 2018, 140:241-251.
[16] Usui N, Fuse M, Hosokawa H, et al. Effects of Hydrogen Peroxide on Radioactive Cobalt Deposition on Stainless Steel Surface in High Temperature Water[J]. Journal of Nuclear Science and Technology, 2005, 42(1):75-81.
[17] Hosokawa H, Nagase M. Investigation of Cobalt Deposition Behavior with Zinc Injection on Stainless Steel under BWR Conditions[J]. Journal of Nuclear Science and Technology, 2004, 41(6):682-689.
[18] Usui N, Fuse M, Hosokawa H, et al. Effects of Hydrogen Peroxide on Cobalt Deposition Rate on Primary Cooling System of Boiling Water Reactors[J]. Journal of Nuclear Science and Technology, 2008, 45(1):72-78.
[19] Fuse M, Nagase M, Usui N, et al. Cobalt Radioactivity Behaviors in a BWR Environment and Countermeasures for Dose Rate Reduction[J]. Nuclear Science and Engineering, 2015, 181(2):175-190.

Figures

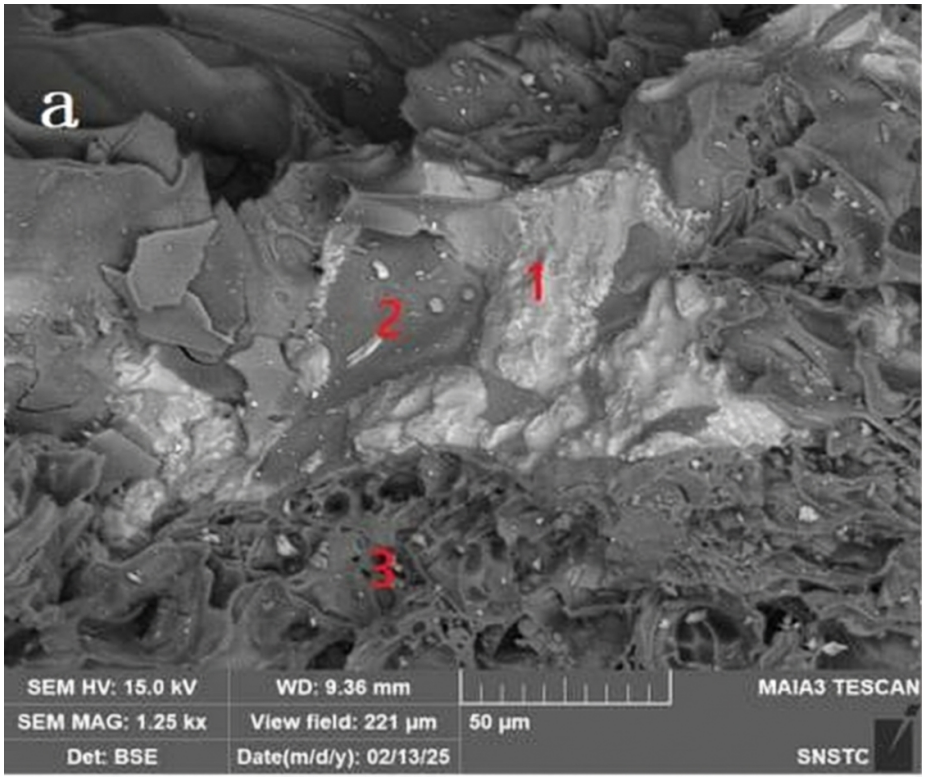

Figure 2: Figure 7